

Magnetic imaging of the pinning mechanism of asymmetric transverse domain walls in ferromagnetic nanowires

Dorothee Petit, Huang T. Zeng, Joao Sampaio, Emma Lewis, Liam O'Brien et al.

Citation: *Appl. Phys. Lett.* **97**, 233102 (2010); doi: 10.1063/1.3523351

View online: <http://dx.doi.org/10.1063/1.3523351>

View Table of Contents: <http://apl.aip.org/resource/1/APPLAB/v97/i23>

Published by the [American Institute of Physics](#).

Related Articles

Domain wall propagation in micrometric wires: Limits of single domain wall regime
J. Appl. Phys. **111**, 07E311 (2012)

Magnetic structure and resonance properties of a hexagonal lattice of antidots
Low Temp. Phys. **38**, 157 (2012)

Thermally activated domain wall dynamics in a disordered magnetic nanostrip
J. Appl. Phys. **109**, 07D345 (2011)

Noise investigation of the orthogonal fluxgate employing alternating direct current bias
J. Appl. Phys. **109**, 07E529 (2011)

Comparison of electrical techniques for magnetization dynamics measurements in micro/nanoscale structures
J. Appl. Phys. **109**, 07D317 (2011)

Additional information on *Appl. Phys. Lett.*

Journal Homepage: <http://apl.aip.org/>

Journal Information: http://apl.aip.org/about/about_the_journal

Top downloads: http://apl.aip.org/features/most_downloaded

Information for Authors: <http://apl.aip.org/authors>

ADVERTISEMENT



ACCELERATE AMBER AND NAMD BY 5X.
TRY IT ON A FREE, REMOTELY-HOSTED CLUSTER.

LEARN MORE

Magnetic imaging of the pinning mechanism of asymmetric transverse domain walls in ferromagnetic nanowires

Dorothee Petit,^{1,a)} Huang T. Zeng,¹ Joao Sampaio,¹ Emma Lewis,¹ Liam O'Brien,¹ Ana-Vanessa Jausovec,¹ Dan Read,¹ Russell P. Cowburn,¹ Kerry J. O'Shea,² Stephen McVitie,² and John N. Chapman²

¹Department of Physics, Nanoscale Magnetics Group, Blackett Laboratory, Imperial College London, Prince Consort Road, London SW7 2BW, United Kingdom

²School of Physics and Astronomy, College of Science and Engineering, University of Glasgow, Glasgow G12 8QQ, United Kingdom

(Received 23 April 2010; accepted 11 November 2010; published online 6 December 2010)

The pinning of asymmetric transverse magnetic domain walls by constrictions and protrusions in thin permalloy nanowires is directly observed using the Fresnel mode of magnetic imaging. Different domain wall (DW)/trap configurations are initialized using *in situ* applied magnetic fields, and the resulting configurations are imaged both at remanence and under applied fields. The nature of the chirality dependent pinning potentials created by the traps is clearly observed. The effect of the asymmetry of the DW is discussed. Micromagnetic simulations are also presented, which are in excellent agreement with the experiments. © 2010 American Institute of Physics.

[doi:10.1063/1.3523351]

A thorough understanding of the interaction between magnetic domain walls (DWs) and artificially engineered defects in nanoscale ferromagnetic wires is greatly desirable from a fundamental point of view and is also of vital importance to a number of DW based logic and memory devices, as well as to related studies such as domain wall (DW)/spin wave interactions¹ or current induced DW motion.^{2,3} Topographical features such as corners, junctions, constrictions, and protrusions in otherwise straight nanostrips allow control of the DWs as they create changes in the energy landscape, which modify the local propagation fields. Switching the field measurements of nanowires containing constrictions and protrusions have recently given rise to a comprehensive description of DW pinning mechanisms.⁴ In particular, the systematic dependency of the pinning energy potential on the chirality of the incoming DW was established. Transverse DWs (TDW) pinned in protrusions and constrictions were recently imaged,^{5,6} but either only one DW chirality or only one type of trap was studied. Here, we use the Fresnel mode of Lorentz transmission electron microscopy to directly image the pinning of TDWs in protrusions and constrictions. The wire dimensions investigated cause asymmetric TDWs (ATDWs) to be pinned. Although the overall pinning mechanism is found to be similar to the one governing the trapping of symmetric TDWs (STDWs) in narrower structures, the asymmetry of the TDW does play a role in the depinning process. The results of micromagnetic simulations are shown in parallel.

The samples were fabricated using electron beam lithography, thermal evaporation of 9 nm thick permalloy, and a lift-off process on top of 50 nm thick Si₃N₄ membranes. Magnetic characterization was carried out using the Fresnel mode of Lorentz microscopy performed in a Philips CM20 FEG TEM suitable for *in situ* magnetizing experiments.⁷ In this microscope, field free imaging conditions are achieved by turning off the objective lens and instead using a pair of

mini-Lorentz lenses situated above and below the objective lens pole pieces. During the *in situ* field-induced DW depinning experiments performed here, the objective lens was weakly excited to provide an out-of-plane field H_z of 48 Oe. The magnitude of the field in the plane of the specimen was varied by tilting the specimen. A maximum tilt angle of 41° was sufficient to completely reverse the wires in this study, which corresponds to a maximum in-plane field of 32 Oe and a H_z of 36 Oe. The structures are 600 nm wide arcs subtending an angle α of 60°, with a radius of curvature $R = 7.5 \mu\text{m}$ measured to the center of the wire [see Fig. 1(a)]. The protrusions and constrictions are semicircles of radius R_{trap} , equal to half the wire width (w), and placed in the middle of the structure. An in-plane magnetic field H_{sat} of ~ 4200 Oe was applied, which saturated the magnetization in both sides of the arc downwards, therefore creating a head to head (HH) TDW with the core magnetization pointing down at the trap. The chirality of the DWs created here, defined by the sense of rotation of the magnetization when going through the DW from left to right, is clockwise. In order to create a DW of opposite chirality, the curvature of the arc should be inverted. However, when studying the interaction of a DW with a trap on one edge of the wire, simple symmetry consideration shows that reversing the chirality of the DW without moving the trap is geometrically equivalent to retaining the chirality of the DW and moving the trap onto the opposite side of the wire.⁴ In this experimental study, we choose to do the latter. The curvature should have negligible effect on the DW pinning at such a large radius of curvature.⁸ TDWs in ferromagnetic nanowires have a characteristic V-shape, uniquely defined by the chirality of the DW. In the case of the TDWs created upon the application of H_{sat} , the wide side is on the outer edge of the arc.

Figure 1 [(d1), (e1), (f1), and (g1)] shows the experimental (top) Fresnel images at remanence after the field-induced DW creation. The Fresnel imaging mode highlights the positions and geometries of the DWs as regions of increased or decreased electron intensity against a neutral

^{a)}Electronic mail: dcmcp2@cam.ac.uk.

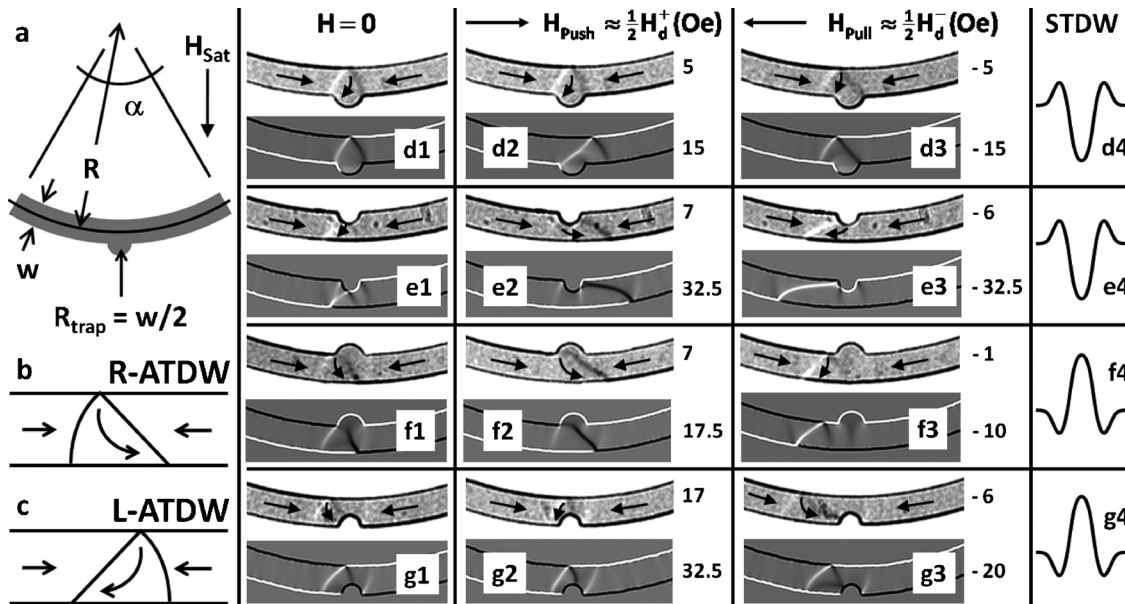


FIG. 1. (a) Schematics of the structures. When H_{Sat} is applied, HHDWs are created at the trap. [(b) and (c)] Schematics of a R- and L-ATDW. [(d)–(g)] Experimental (top) and simulated (bottom) Fresnel images. (d1), (e1), (f1), and (g1) are taken at remanence after the field-induced DW creation. (d2), (e2), (f2), (g2), (d3), (e3), (f3), and (g3) are taken under magnetic field. The small arrows indicate the directions of the magnetization in the structure. The profiles used for the simulations were obtained using images of the real structures. (d4), (e4), (f4), and (g4) show the potential profiles obtained for STDWs (Ref. 5).

background. Intensity variations, referred to as fringes, also arise at the structure edges resulting from both the magnetic and electrostatic contributions. The fringe at one edge of the wire is thicker as a result of the asymmetric deflection of electrons by the Lorentz force and is indicative of the direction of magnetization in the wire. An ATDW (Ref. 9) is so called due to the magnetization curling in one direction (right, R, or left, L), breaking the left-right symmetry [Figs. 1(b) and 1(c)]. In this work, we consider both the effect of the chirality of the DW and the effect of the R-/L-asymmetry. Experimentally, the type of ATDW created cannot be controlled but it can be recognized by observing the contrast at the wire edge. In (d1), for example, the thick dark fringe that runs along the lower edge of the wire to the right of the TDW and continues along the edge of the protrusion indicates that the DW is a L-HHDW. The fact that we observe TDWs at these dimensions where vortex DWs are the stable configuration is attributed to the metastability of the transverse state in which the DWs are initially created.¹⁰ Below, each experimental image is the corresponding calculated Fresnel image obtained from the micromagnetic configurations simulated using the OOMMF package¹¹ and with the profiles obtained using the scanning electron microscope images of the structures ($M_S=8 \times 10^5$ A/m, $A=13 \times 10^{-12}$ J/m, $\alpha=0.5$, and cell size= $5 \times 5 \times 9$ nm³). All simulated depinning fields discussed in this paper were obtained with these simulations on the “real” structures. In order to differentiate the effect of the DW asymmetry from the effect of the other sources of asymmetry, such as random defects in the structure or misalignment of the arc with the applied field, straight, smooth, and perfectly symmetrical structures of identical dimensions (referred to as “perfect” structures), were also simulated. The perfect structures gave qualitatively identical results to the real ones. The out-of-plane component H_z of the applied field present in the experiments was included in one case and found to have no effect on the depinning field. Fresnel images were calculated

from the magnetic contribution only, ignoring electrostatic effects, and as a result, some differences in contrast appear along the wire edges, for example, the bright white line appearing along the wire edge in the calculated image does not appear in the experimental image due to the additional superimposed electrostatic contribution. As expected, a downward HHDW is seen to experience different potential landscapes in the vicinity of the different trap configurations: in (d1) and (e1), the equilibrium position of the ATDW is close to the middle of the trap, while in (f1) and (g1), it ends up at the side of the trap, in agreement with the potential profiles expected for STDWs (Ref. 4) and shown in (d4), (e4), (f4), and (g4). However, because of the asymmetry of the TDW, remanence images are not enough to conclude on the nature of the potential. In Fig. 1 [(d2), (e2), (f2), and (g2)], a positive horizontal magnetic field H_{Push} of the order of $H_d^+/2$ is applied, where H_d^+ is the depinning field (experimental or simulated) in the positive direction for each particular configuration. (d3), (e3), (f3), and (g3) are obtained, as a magnetic field H_{Pull} of the order of $H_d^-/2$ is applied in the negative direction, where H_d^- is the depinning field in the negative direction. The values of H_{Push} and H_{Pull} are indicated next to each picture. The qualitative agreement between the experimental and calculated Fresnel images is excellent. No quantitative agreement between room temperature experimental switching fields and zero temperature simulated switching fields is expected.¹²

In (d), the depinning fields were measured at $H_d^+ = 10 \pm 0.5$ Oe/ $H_d^- = -9.2 \pm 0.5$ Oe. They were calculated at $\pm 27.5 \pm 2.5$ Oe. The simulations performed on the perfect structures show that both R- and L-ATDWs are pinned in the middle of the trap and that the depinning fields depend on the DW type. In that case, the top narrow side of the DW is more free to move than the bottom wide side, and the leading edge of the DW during depinning is the narrow side. When a R-ATDW is pushed to the right, it simultaneously transforms into a L-ATDW (the leading edge of which is the narrow

side) and depins at a higher field than when pulled. The potential that an ATDW experiences is an asymmetric well. In (d2) and (d3), a L-ATDW is seen to deform as its bottom wide side is pinned at the protrusion, while its top narrow side extends away from the trap. No asymmetry was detected in the pinning strength within the precision of the applied field. During the experiment, the out-of-plane component of the field at $H_d^+ = 10$ Oe was $H_z = 47$ Oe. In order to assess the effect of such a high out-of-plane field on the depinning field, the same simulations were run with $H_z = 130$ Oe (the simulated value of H_z was scaled to the simulated value of H_d^+). H_d^+ was still 27.5 ± 2.5 Oe.

In (e), the depinning fields were measured at $+12.5 \pm 0.6$ Oe/ -10.8 ± 0.5 Oe. They were calculated at $\pm 70 \pm 10$ Oe. Both simulations and experiments show that the bottom wide side of the DW is more free to move than the top narrow side so that the leading side of the DW as it leaves the trap in either direction is the wide side. If the wide side of the DW is not on the appropriate side initially (as in the case of a L-ATDW being pushed toward the right, for instance), the DW first transforms. In other words, the field H_c required to change the ATDW type is lower than the depinning field. The positive and negative depinning fields are the same, as expected from simple symmetry considerations above H_c . Figure 1 [(e1)], shows a L-ATDW at remanence. In (e2), this DW has transformed into a R-ATDW as it is pushed using a field above H_c . In (e3), a L-ATDW is pulled toward the left.

In (f), the depinning fields were measured at $+14.1 \pm 0.7$ Oe/ -2.1 ± 0.4 Oe; they were calculated at $+35 \pm 5$ Oe/ -25 ± 5 Oe. In this case, the DW is always pinned in the side of the trap (f1). This fact, together with a direction-dependent depinning field, is characteristic of a potential barrier. The non-negligible value of H_d^- indicates the presence of side wells. Both simulations and experiments show that as the DW is pushed through the barrier, the bottom wide side of the DW is more free to move than the top narrow side, and the leading edge of the DW is the wide side. As in case (e), the field at which the ATDW transforms into the appropriate type is smaller than H_d^+ . When pulled out of the side well, the simulations on the perfect structures show that both types of DW depin at the same field, keeping their structure. In (f2), the R-ATDW created in (f1) remains trapped on the left side of the protrusion as it is pushed toward the right (against the central barrier), whereas in (f3), the L-ATDW (created in a subsequent run) is seen to be trapped on the left side of the protrusion as the field is reversed (side well).

In (g), finally, the depinning fields were measured at $+31.6 \pm 1.5$ Oe/ -11.2 ± 0.5 Oe. They were calculated at $>+65 \pm 5$ Oe/ -36 ± 4 Oe. In that case also, the DW experiences a potential barrier with side wells. The simulations on the perfect structures show that any type of DW initialized in the vicinity of such a trap ends up on the side of the trap and in a configuration such that its core magnetization points

toward the trap. If a DW is artificially created with its core magnetization pointing away (L-ATDW on the left for instance), it spontaneously transforms into the appropriate kind ($H_c = 0$) so that an ATDW always has its core magnetization aligned with the applied field when pushed past the main barrier and antialigned when pulled away from the side well. In (g2), a R-ATDW is compressed against the barrier under a positive field; in (g3), one side of it remains attached to the side of the trap, while it extends as the field is reversed to pull it away from the side well.

In conclusion, we have studied the depinning of ATDWs from protrusions and constrictions both experimentally using the Fresnel imaging technique and by means of micromagnetic simulations. All possible trap/DW configurations are clearly imaged. The asymmetry of the DW is found to cause only small modifications to the potential disruption found for STDWs by indirect measurements,⁵ and as shown in Fig. 1 [(d4), (e4), (f4), and (g4)], the main features of the potential are preserved (well or barrier). However, when pinned by protrusions or constrictions placed on one side of the nanowire, one side of the DW (wide or narrow) is pinned more strongly than the other, the latter being more free to move. This leads to the possibility that an ATDW of a given type transforms into the other type if its leading edge is not the appropriate one for the given direction of movement and if the field required for this transformation is smaller than the depinning field.

This work was supported by the European Community under the Sixth Framework Programme SPINSWITCH (Grant No. MRTN-CT-2006-035327).

- ¹C. W. Sandweg, S. J. Hermsdoerfer, H. Schultheiss, S. Schafer, B. Leven, and B. Hillebrands, *J. Phys. D* **41**, 164008 (2008).
- ²J. Grollier, D. Lacour, V. Cros, A. Hamzic, A. Vaures, A. Fert, D. Adam, and G. Faini, *J. Appl. Phys.* **92**, 4825 (2002).
- ³C. K. Lim, T. Devolder, C. Chappert, J. Grollier, V. Cros, A. Vaurès, A. Fert, and G. Faini, *Appl. Phys. Lett.* **84**, 2820 (2004).
- ⁴D. Petit, A.-V. Jausovec, D. Read, and R. P. Cowburn, *J. Appl. Phys.* **103**, 114307 (2008).
- ⁵C. W. Sandweg, N. Wiese, D. McGrouther, S. J. Hermsdoerfer, H. Schultheiss, B. Leven, S. McVitie, B. Hillebrands, and J. N. Chapman, *J. Appl. Phys.* **103**, 093906 (2008).
- ⁶K. He, D. J. Smith, and M. R. McCartney, *Appl. Phys. Lett.* **95**, 182507 (2009).
- ⁷J. N. Chapman, A. B. Johnston, L. J. Heyderman, S. McVitie, W. A. P. Nicholson, and B. Bormans, *IEEE Trans. Magn.* **30**, 4479 (1994).
- ⁸E. R. Lewis, D. Petit, L. Thevenard, A. V. Jausovec, L. O'Brien, D. E. Read, and R. P. Cowburn, *Appl. Phys. Lett.* **95**, 152505 (2009).
- ⁹Y. Nakatani, A. Thiaville, and J. Miltat, *J. Magn. Magn. Mater.* **290–291**, 750 (2005).
- ¹⁰M. Laufenberg, D. Backes, W. Buhner, D. Bedau, M. Klau, U. Rudiger, C. A. F. Vaz, J. A. C. Bland, L. J. Heyderman, F. Nolting, S. Cherifi, A. Locatelli, R. Belkhou, S. Heune, and E. Bauer, *Appl. Phys. Lett.* **88**, 052507 (2006).
- ¹¹The oommf code is available at <http://math.nist.gov/oommf>.
- ¹²A. Himeno, T. Okuno, T. Ono, K. Mibu, S. Nasu, and T. Shinjo, *J. Magn. Magn. Mater.* **286**, 167 (2005).